applied sciences

MDPI

Article

Slip Flow and Heat Transfer of Nanofluids over a Porous Plate Embedded in a Porous Medium with Temperature Dependent Viscosity and Thermal Conductivity

Sajid Hussain [1], Asim Aziz [2,*], Taha Aziz [3] and Chaudry Masood Khalique [3]

1 Department of Mathematics, Capital University of Science and Technology, Islamabad 44000, Pakistan; prsajid@yahoo.com
2 College of Electrical and Mechanical Engineering, National University of Sciences and Technology, Rawalpindi 46070, Pakistan
3 International Institute for Symmetry Analysis and Mathematical Modeling, Department of Mathematical Sciences, North-West University, Mafikeng Campus, Private Bag X 2046, Mmabatho 2735, South Africa; tahaaziz77@yahoo.com (T.A.); Masood.Khalique@nwu.ac.za (C.M.K.)
* Correspondence: aaziz@ceme.nust.edu.pk; Tel.: +92-3325-464-647

Academic Editor: Rahmat Ellahi
Received: 20 September 2016; Accepted: 3 November 2016; Published: 14 December 2016

Abstract: It is well known that the best way of convective heat transfer is the flow of nanofluids through a porous medium. In this regard, a mathematical model is presented to study the effects of variable viscosity, thermal conductivity and slip conditions on the steady flow and heat transfer of nanofluids over a porous plate embedded in a porous medium. The nanofluid viscosity and thermal conductivity are assumed to be linear functions of temperature, and the wall slip conditions are employed in terms of shear stress. The similarity transformation technique is used to reduce the governing system of partial differential equations to a system of nonlinear ordinary differential equations (ODEs). The resulting system of ODEs is then solved numerically using the shooting technique. The numerical values obtained for the velocity and temperature profiles, skin friction coefficient and Nusselt's number are presented and discussed through graphs and tables. It is shown that the increase in the permeability of the porous medium, the viscosity of the nanofluid and the velocity slip parameter decrease the momentum and thermal boundary layer thickness and eventually increase the rate of heat transfer.

Keywords: nanofluids; variable viscosity; variable thermal conductivity; partial slip; heat transfer; porous plate

1. Introduction

The heat transfer due to fluid flow is an important factor in problems in industries, such as heat exchangers, the recovery of petroleum resources, fault zones, catalytic reactors, cooling systems, electronic equipment manufacturing, etc. The heat transfer characteristics in the boundary layer are influenced by a number of factors, including flow geometry, the viscosity of a fluid, thermal conductivity, bounding surface characteristics, boundary conditions, flow medium and the orientation and intensity of the applied magnetic field [1–3]. Maxwell first proposed that the thermal conductivity of the fluid can be increased by including solid particles in the flow domain [4]. Following Maxwell, extensive research has been conducted to study the heat transfer characteristics of fluid flow in a porous medium. It is beyond the scope of this work to revisit the vast amount of literature on

different Newtonian and non-Newtonian fluids' flow within a porous medium. A comprehensive literature on forced/natural convective heat transfer in porous medium can be found in [5,6].

The introduction of nanofluids by Choi [7] offered new possibilities of heat transfer enhancement, and a number of studies were conducted to study the effects of the thermal properties (mainly thermal conductivity), viscosity and convective heat transfer performance of nanofluids. Experiments performed by Wang et al. [8] and Keblinski et al. [9] showed that the effective thermal conductivity of nanofluids increases under macroscopically stationary conditions. Buongiorno [10] performed a detailed analysis on convective transport in nanofluids. A comprehensive literature survey on transport and heat transfer characteristics of nanofluids was presented in the review articles of Keblinski et al. [11] and Wang and Mujumdar [12]. It has been demonstrated that nanofluids can have significantly better heat transfer characteristics than the conventional fluids depending upon the type, size and concentration of nanoparticles and the nanofluids' transport through the porous media.

Nield and Kuznetsov [13,14] first studied the effects of porous media, thermophoresis and Brownian motion on the convective heat transfer of nanofluids. Sun and Pop [15] found the numerical solution of the steady-state free convection heat transfer behavior of nanofluids inside a triangular enclosure saturated by a porous media. It was observed that the heat transfer rate increases with the increase in nanoparticle volume concentration at a low Rayleigh number, whereas the opposite trend was observed for a high Rayleigh number. Khan and Aziz [16] studied the double-diffusive free convection from a vertical plate to a porous medium saturated with a binary base nanofluid. The influence of the internal heat source on the onset of Darcy–Brinkman convection in a porous layer filled with a nanofluid was presented by Yadav et al. [17]. They showed that the porous medium has stabilizing effects on the modeled system. Khan et al. [18] studied the free convection of nanofluids along a vertical plate in porous media. Servati et al. [19] studied numerically the force convective MHDflow of a nanofluid in a channel partially filled with porous media. The steady mixed convection boundary layer flow of nanofluids past a vertical flat plate embedded in porous media was discussed by Ahmad and Pop [20]. Recently, Cimpean and Pop [21] presented a detailed study on the flow of three different nanofluids ($Cu-$water,Al_2O_3-water and TiO_2-water) in an inclined channel saturated by a porous media. A review article detailing the literature on the convective heat transfer of nanofluids in porous media and some recent investigations on nanofluids models and related topics can be found in [22–26].

It can be seen from the available literature that limited or no attention has been given to the slip wall condition and the effects of variable thermophysical properties on the flow and heat transfer characteristics of nanofluids. Wall slip has far-reaching implications for many branches of science, engineering and industry. These include rheometric measurements, material processing and fluid transportation [27,28]. Moreover, many processes in engineering occur at high temperature, and it is well known that the thermophysical properties of fluids may change with temperature and become important for the design of reliable equipment, nuclear plants, gas turbines and various propulsion devices or aircraft, missiles, satellites and space vehicles. On the basis of these applications, Khan et al. [29] studied the flow and heat transfer of carbon nanotubes (CNTs) subjected to Navier slip and uniform heat flux boundary conditions. Zheng et al. [30] extended the idea and studied the effects of velocity slip and temperature jump on MHD flow and heat transfer of nanofluids over a porous shrinking sheet. Moreover, Zhenga et al. [31] presented an investigation for the flow and radiation heat transfer of a nanofluid over a porous sheet with velocity slip and temperature jump in a porous medium. Uddin et al. [32] analyzed numerically the g-Jittermixed convective unsteady slip flow of nanofluids past a permeable linear porous sheet embedded in a Darcian porous media with variable viscosity. Noghrehabadi et al. [33] observed the effects of partial slip boundary conditions on the flow and heat transfer of nanofluids. Bhaskar et al. [34] carried out an analysis to investigate the influence of variable thermal conductivity and partial velocity slip on the hydromagnetic two-dimensional boundary layer flow of nanofluids over a porous sheet with a convective boundary condition. Noghrehabadi et al. [35] carried out a study on the effects of variable thermal conductivity and viscosity on the natural

convective heat transfer of nanofluids over a vertical plate. Comprehensive studies and lists of important references on the wall slip condition and variable thermophysical properties of nanofluids are presented in [36–41].

In the present work, a mathematical model is presented to study the effects of partial slip, variable viscosity and variable thermal conductivity on steady boundary layer flow of a nanofluid over a porous sheet in a Darcy-type porous medium. The wall slip conditions are employed in terms of shear stress, with viscosity and thermal conductivity as linear functions of temperature. Similarity solutions are obtained, and the reduced system of ordinary differential equations is solved numerically using the shooting method. The numerical results obtained for the velocity and temperature profiles are influenced appreciably by the presence of variable viscosity, variable thermal conductivity, porous medium, velocity and temperature slip and suction/injection parameters. The effects of various parameters on velocity and temperature profiles, as well as skin friction and the rate of heat transfer are presented and discussed through graphs and tables.

2. Mathematical Model of the Problem

We consider the steady two-dimensional laminar boundary layer flow with heat transfer of an incompressible nanofluid over a semi-infinite porous plate in a porous medium. The surface of the plate is at constant temperature T_w and admits the partial slip condition. The viscosity and the thermal conductivity of the nanofluid are considered to vary linearly with temperature. The x-axis is along the surface of the plate, and the y-axis is perpendicular to it. All body forces are neglected, and there is a constant suction/injection velocity V_w at the surface of the plate. The flow far away from the plate is uniform and in the direction parallel to the plate. The velocity and temperature outside the boundary layer are u_∞ and T_∞, respectively. The geometry of the flow model is given in Figure 1.

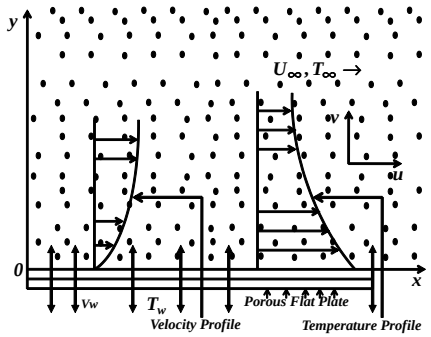

Figure 1. Schematic representation of the geometry.

In view of the above assumptions, the continuity, momentum and energy equations for the flow along with heat transfer are:

$$\frac{\partial u}{\partial x} + \frac{\partial v}{\partial y} = 0, \tag{1}$$

$$u\frac{\partial u}{\partial x} + v\frac{\partial u}{\partial y} = \frac{1}{\rho_{n_f}}\frac{\partial}{\partial y}\left[\mu_{n_f}(T)\frac{\partial u}{\partial y}\right] - \frac{\mu_{n_f}(T)}{\rho_{n_f}k}(u - u_\infty), \tag{2}$$

$$u\frac{\partial T}{\partial x} + v\frac{\partial T}{\partial y} = \frac{1}{(\rho C_p)_{n_f}}\frac{\partial}{\partial y}\left[\kappa_{n_f}(T)\frac{\partial T}{\partial y}\right]. \tag{3}$$

In the above system of equations, u and v represent velocities in the x and y directions, respectively; k is the permeability of the medium; T is the nanofluid temperature; $\mu_{n_f}(T)$ the nanofluid temperature-dependent viscosity; ρ_{n_f} the nanofluid density; $(C_p)_{n_f}$ is the specific heat at constant pressure; and $\kappa_{n_f}(T)$ is the thermal conductivity of the nanofluid.

The appropriate partial slip boundary conditions for velocity and temperature are:

$$u = L_1 \frac{\partial u}{\partial y}, \quad v = V_w \quad \text{at} \quad y = 0; \quad u \to u_\infty \quad \text{as} \quad y \to \infty, \tag{4}$$

$$T = T_w + D_1 \frac{\partial T}{\partial y} \quad \text{at} \quad y = 0; \quad T \to T_\infty \quad \text{as} \quad y \to \infty. \tag{5}$$

Here, $L_1 = LR_{e_x}$ is the velocity slip factor, and $D_1 = D\sqrt{LR_{e_x}}$ is the thermal slip factor with L and D the initial values of velocity and thermal slip factors; and $R_{e_x} = \frac{u_\infty x}{\nu_f}$ is the local Reynolds's number with $\nu_f = \frac{\mu_f}{\rho_f}$ the kinematic viscosity of the base fluid. V_w shows the mass transfer at the surface with $V_w > 0$ for injection and $V_w < 0$ for suction.

Following Maxwell [4], Bhaskar et al. [34] and Arunachalam [42], the nanofluid's physical parameters are taken as:

$$\rho_{n_f} = (1 - \phi\rho_f + \rho_s), \qquad (\rho C_p)_{n_f} = (1 - \phi(\rho C_p)_f + \phi(\rho C_p)_s), \tag{6}$$

$$\mu_{nf} = \mu^*_{n_f}\left[a + b(T_w - T)\right], \qquad \kappa_{nf}(T) = \kappa^*_{n_f}\left[1 + \epsilon\frac{T - T_\infty}{T_w - T_\infty}\right], \tag{7}$$

$$\mu^*_{n_f} = \mu_f(1 - \phi)^{-2.5}, \qquad \frac{\kappa^*_{n_f}}{\kappa_f} = \frac{(\kappa_s + 2\kappa_f) - 2\phi(\kappa_f - \kappa_s)}{(\kappa_s + 2\kappa_f) + \phi(\kappa_f - \kappa_s)}. \tag{8}$$

In Equations (6)–(8), ϕ is the nanoparticle volume fraction coefficient, ρ_f the density of the base fluid, ρ_s the density of the nanoparticles, $(Cp)_f$ the specific heat capacity of the base fluid, $(Cp)_s$ the specific heat capacity of the nanoparticles, $\mu^*_{n_f}$ and $\kappa^*_{n_f}$ the constant values of the coefficient of viscosity and thermal conductivity of the nanofluid, respectively, and a, b and ϵ the constants with $b > 0$, μ_f, κ_f and κ_s the coefficient of viscosity, thermal conductivity of base fluid and nanoparticles, respectively.

3. Solution of the Problem

We introduce the relation for u, v and T as:

$$u = \frac{\partial \psi}{\partial y}, \qquad v = -\frac{\partial \psi}{\partial x}, \qquad \theta(\eta) = \frac{T - T_\infty}{T_w - T_\infty}, \tag{9}$$

where the stream function $\psi(\eta)$ and dimensionless similarity variable η are defined by (see, for example, Bhattacharyya et al. [43])

$$\psi = \nu_f R_{e_x}^{\frac{1}{2}} f(\eta), \qquad \eta = \frac{y}{x} R_{e_x}^{\frac{1}{2}}. \tag{10}$$

Equations (9) and (10) together with Equations (6)–(8) reduce the boundary value problem (2)–(5) to:

$$(a + A - A\theta)f''' + (1 - \phi)^{2.5}(1 - \phi + \phi\frac{\rho_s}{\rho_f})(\frac{1}{2}ff'') - A\theta' f'' - k^*(a + A - A\theta)(f' - 1) = 0, \tag{11}$$

$$(1 + \epsilon\theta)\theta'' + \epsilon\theta'^2 + P_r(\frac{k_f}{k_{n_f}})\left(1 - \phi + \phi\frac{(\rho C_p)_s}{(\rho C_p)_f}\right)\left(\frac{1}{2}f\theta'\right) = 0, \tag{12}$$

$$f(\eta) = S, \quad f'(\eta) = \delta f''(\eta) \quad \text{at} \quad \eta = 0; \quad f'(\eta) \to 1 \quad \text{as} \quad \eta \to \infty \tag{13}$$

$$\theta(\eta) = 1 + \Delta\theta'(\eta) \quad \text{at} \quad \eta = 0; \quad \theta(\eta) \to 0 \quad \text{as} \quad \eta \to \infty, \tag{14}$$

where $A = b(T_w - T_\infty)$ is the viscosity parameter, $k^* = \frac{1}{D_{a_x} R_{e_x}}$ is the permeability parameter, $D_{a_x} = \frac{k}{x^2}$ is the local Darcy number, $P_r = \frac{\nu_f}{\alpha_f}$ is the Prandtl number, $\alpha_f = \frac{k_f}{(\rho C_p)_f}$ is the diffusivity parameter, ϵ is the thermal conductivity parameter, $\delta = \frac{Lu_\infty}{\nu_f}$ is the velocity slip parameter and $\Delta = \frac{Du_\infty}{\nu_f}$ is the thermal slip parameter.

The important physical quantities of interest are the skin friction coefficient C_F (rate of shear stress) and the local Nusselt number N_{u_x} (rate of heat transfer at the surface). The skin friction coefficient and the Nusselt number are defined as:

$$C_F = \frac{\tau_w}{\rho U_w^2}, \qquad N_{u_x} = \frac{x q_w}{k_f (T_w - T_\infty)}, \tag{15}$$

where the local wall shear stress τ_w and the heat transfer from the plate q_w are given by:

$$\tau_w = -\mu_{n_f} (\frac{\partial u}{\partial y})_{y=0}, \qquad q_w = \kappa_{n_f} (\frac{\partial T}{\partial y})_{y=0} \tag{16}$$

with u the flow velocity parallel to the porous plate and y the distance to the plate. Using Equation (16), the dimensionless forms of Equation (15) become:

$$C_f R_{e_x}^{1/2} (1-\phi)^{2.5} = -f''(0), \qquad N_{u_x} R_{e_x}^{-1/2} (\frac{k_f}{k_{n_f}}) = -\theta'(0). \tag{17}$$

4. Numerical Method for Solution

The nonlinear coupled ordinary differential Equations (11) and (12) subject to boundary conditions (13) and (14) form the two-point boundary value problem and are solved numerically using the shooting method. In order to use the shooting method, first we convert (11) and (12) to a system of first order differential equations:

$$f' = p, \quad p' = q, \quad \theta' = z, \tag{18}$$

$$q' = \frac{1}{(a + A - A\theta)} \left[(1-\phi)^{2.5} (1 - \phi + \phi \frac{\rho_s}{\rho_f}) (-\frac{1}{2} f q) + A z q + k^* (a + A - A\theta)(p-1) \right], \tag{19}$$

$$z' = \frac{1}{(1+\epsilon\theta)} \left[-\epsilon z^2 - P_r (\frac{k_f}{k_{n_f}}) \left(1 - \phi + \phi \frac{(\rho C_p)_s}{(\rho C_p)_f} \right) \left(\frac{1}{2} f z \right) \right]. \tag{20}$$

The boundary conditions become:

$$f(0) = S, \quad p(0) = 1 + \delta q(0), \quad \theta(0) = 1 + \Delta z(0). \tag{21}$$

In order to solve the initial value problem (19)–(21) with the shooting method, we require an initial guess for $q(0)$ and $z(0)$. The required values of $q(0)$ and $z(0)$ are chosen randomly, and numerical solutions are obtained using fourth order Runge–Kutta method. The numerical values for $q(0)$ and $z(0)$ are adjusted using Newton's method to give better approximation to the solution. The step size is taken as 0.01, and the process is repeated until the solutions achieve the accuracy of 10^{-6}. To ensure the numerical accuracy, we have compared our results with the results of Bhattacharyya et al. [43] for velocity and temperature profiles with $A = \epsilon = \phi = 0, a = 1, S = 0.2, \delta = \Delta = 0.1$ and $P_r = 0.3$. The comparison is shown in Figure 2 and is found to be in excellent agreement.

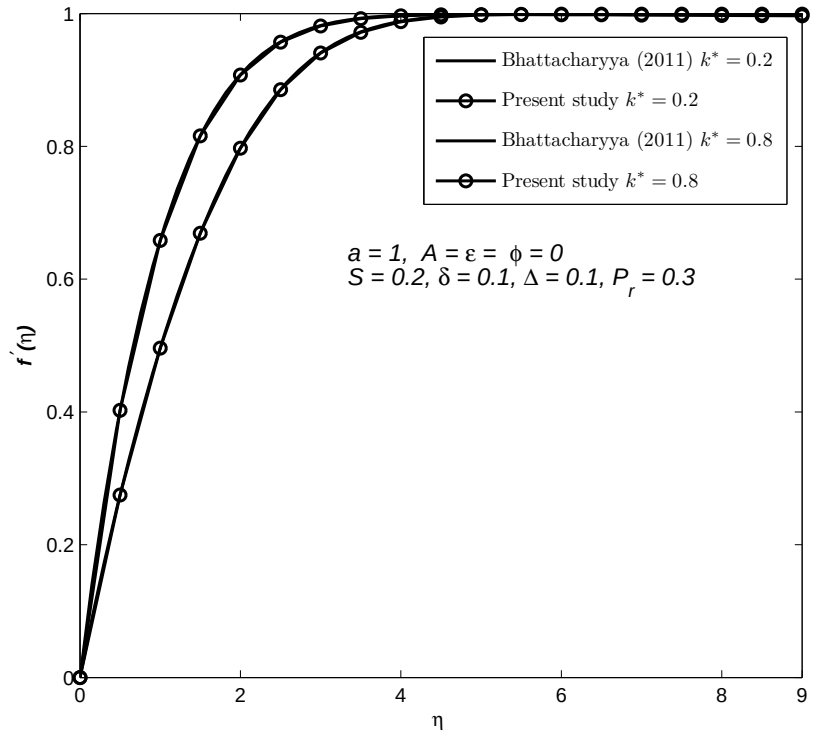

Figure 2. Comparison of the results for the velocity $f'(\eta)$ profiles for different values of permeability parameter k^*, with Bhattachaaya et al. [43].

The thermophysical properties of the base fluid and nanoparticles are given in Table 1

Table 1. Thermophysical properties of base fluid and nanoparticles [44].

Physical Properties	Units	Base Fluid Water	Nanoparticles (Solid) Cu (300-K)
Density ρ	(kg/m^3)	997.1	8933
Specific heat Cp	(J/kg·K)	4179	385
Thermal conductivity κ	(W/m·K)	0.613	401

5. Numerical Results and Discussion

In this section, the numerical results calculated for the velocity and temperature profiles are presented through graphs and tables. The computations are performed to study the effects of the variation of permeability parameter k^*, nanofluid volume concentration parameter ϕ, velocity slip parameter δ, thermal slip parameter Δ, suction and injection parameter S, viscosity parameter A and variable thermal conductivity ϵ on the velocity and temperature profiles of the Cu-water nanofluid. The behavior of the skin friction coefficient and Nusselt number with the variation in physical parameters is also shown in Table 2.

Table 2. Values of skin friction $= -f''(0)$ and Nusselt number $= -\theta'(0)$.

κ^*	A	ϕ	ϵ	S	δ	Δ	$-f''(0)$	$-\theta'(0)$
$a = 1$								
0.2	0.2	0.2	0.3	0.2	0.1	0.1	0.5844	0.2513
0.8							0.9158	0.2678
0.1	0.2	0.2	0.3	0.1	0.1	0.1	0.6139	0.6594
0.4							0.8145	0.6951
0.9							1.0470	0.7290
0.4	0.1	0.2	0.3	0.1	0.1	0.1	0.7858	0.7996
	0.6						0.8780	0.8098
	1.5						1.0186	0.8239
0.4	0.2	0.0	0.3	0.1	0.1	0.1	0.7815	0.9284
		0.05					0.7880	0.8621
		0.2					0.8145	0.6951
0.4	0.2	0.2	0.1	0.1	0.1	0.1	0.8158	0.7709
			0.4				0.8139	0.6639
			0.8				0.8115	0.5693
0.4	0.2	0.2	0.3	0.1	0.1	0.1	0.7742	0.6135
				0.2			0.8145	0.6951
				0.3			0.8553	0.7794
0.4	0.2	0.2	0.3	0.2	0.1	0.1	0.8145	0.6951
					0.3		0.7163	0.7404
					0.6		0.6007	0.7869
0.4	0.2	0.2	0.3	0.2	0.1	0.1	0.8145	0.6951
						0.3	0.8052	0.6188
						0.6	0.7949	0.5292

The influence of the permeability parameter k^* on the velocity and temperature profiles in the presence of slip at the boundary is depicted in Figures 3 and 4. The velocity and temperature profiles are plotted for several values of permeability parameter k^* for the Cu-water nanofluid. It is observed that the velocity of the nanofluid increases with the increase in the permeability of the medium and consequently decreases the thickness of the momentum boundary layer. This is due to the fact that the increase in permeability reduces the magnitude of the Darcian body force (inversely proportional to the permeability) and enhances the motion of the fluid in the boundary layer. In other words, progressively less drag is experienced by the flow, and flow retardation thereby decreases. From Figure 4, it is noticed that the temperature $\theta(\eta)$ at a fixed distance from the plate decreases with the increase in k^*. The permeability parameter is inversely proportional to the density of the base fluid, hence the increase in k^* causes a decrease in the density and temperature of the nanofluid within the boundary layer. In conclusion, the increase in the permeability of the porous medium decreases the thickness of momentum and thermal boundary layers and eventually increases the heat transfer rate.

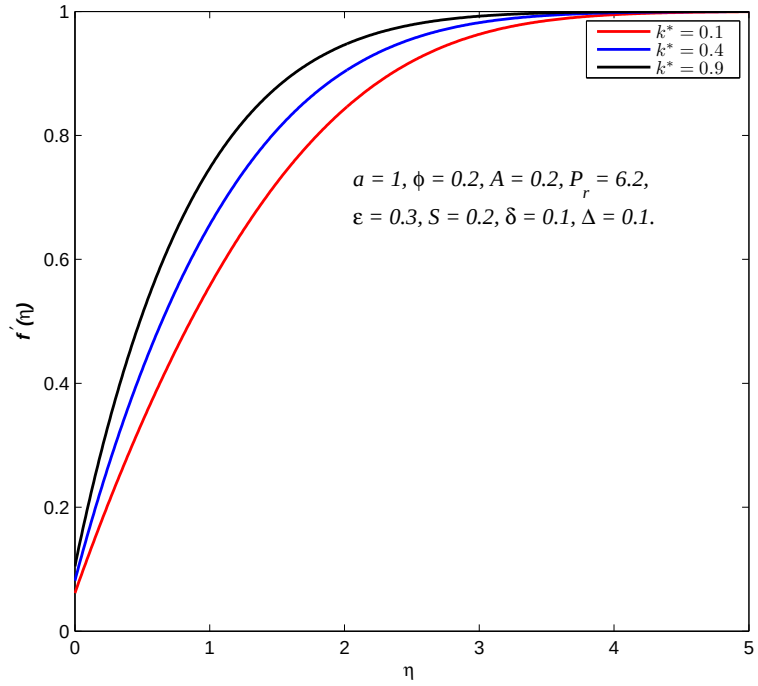

Figure 3. Velocity $f'(\eta)$ profiles for different values of permeability parameter k^*.

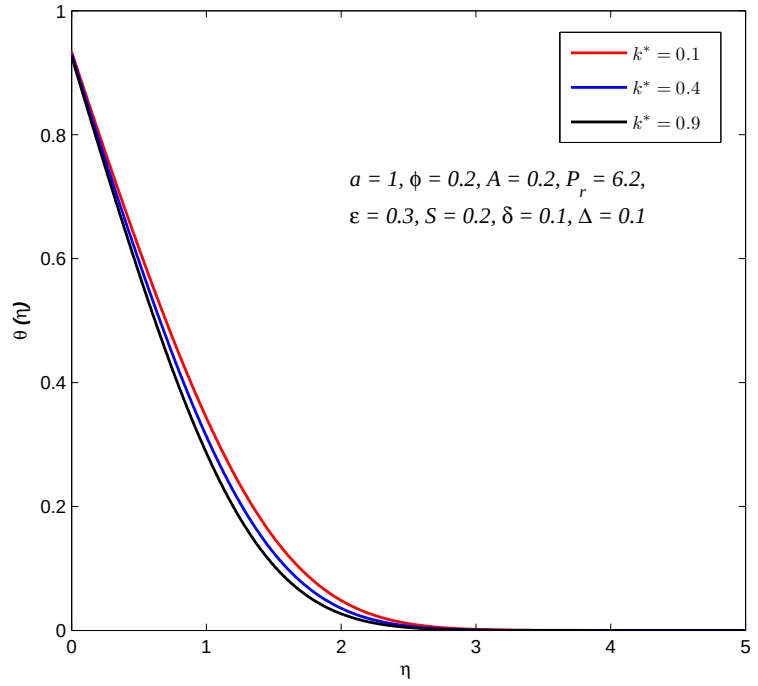

Figure 4. Temperature $\theta(\eta)$ profiles for different values of permeability parameter k^*.

The effect of nanoparticle volume concentration parameter ϕ on the velocity and temperature profiles of the Cu-water nanofluid is shown in Figures 5 and 6. It is observed that the velocity of the fluid decreases, whereas the temperature of the nanofluid increases with the increase in volume

concentration parameter ϕ. This illustrates the agreement with the physical behavior of the nanofluids, i.e., the increase in the volume of nanoparticles causes an increase in the thermal conductivity of the fluid, which leads to the increase in the thickness of the thermal boundary layer.

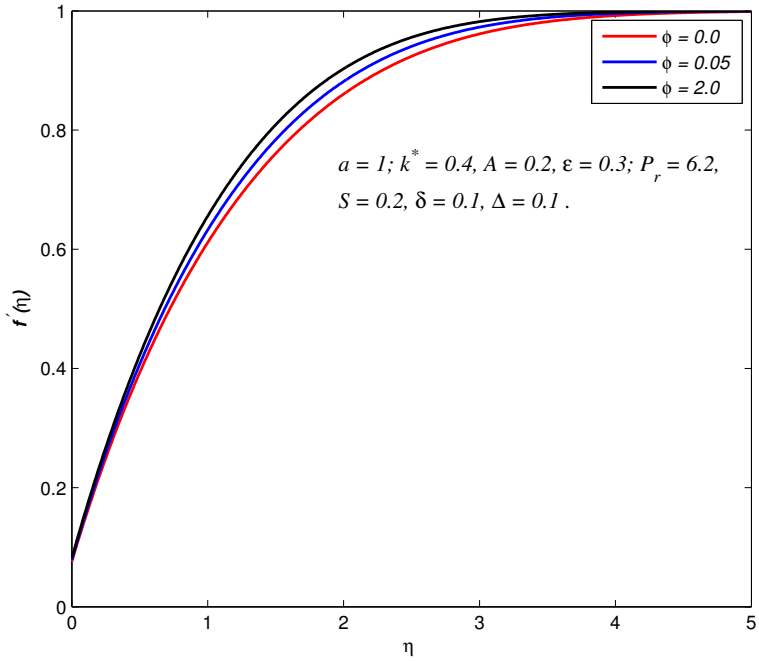

Figure 5. Velocity $f'(\eta)$ profiles for different values of volume fraction coefficient ϕ.

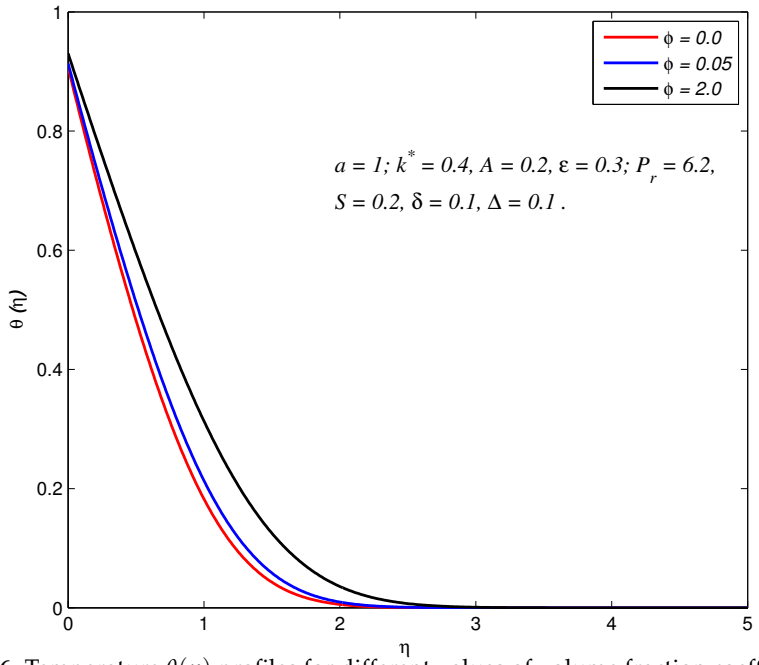

Figure 6. Temperature $\theta(\eta)$ profiles for different values of volume fraction coefficient ϕ.

Figures 7 and 8, respectively, show the nanofluid velocity and temperature profiles for different values of viscosity parameter A. The comparison of curves in Figure 7 shows that the velocity of the nanofluid initially increases with the increase in viscosity parameter A. This increase in velocity corresponds to a reduction in the thickness of the momentum boundary layer. Moreover, the cross-over point is also observed for velocity profiles in Figure 7. The velocity profiles exhibit opposite behaviors after crossing the cross-over point, that is the velocity decreases with the increasing values of viscosity

parameter A after the crossing-over point. This corresponds to an increase in the thickness of the boundary layer. It is observed from Figure 8 that the increase in the viscosity parameter enhances the heat transfer rate and decreases the thickness of the thermal boundary layer. The impact of A on the velocity profiles is more pronounced than on the temperature profiles.

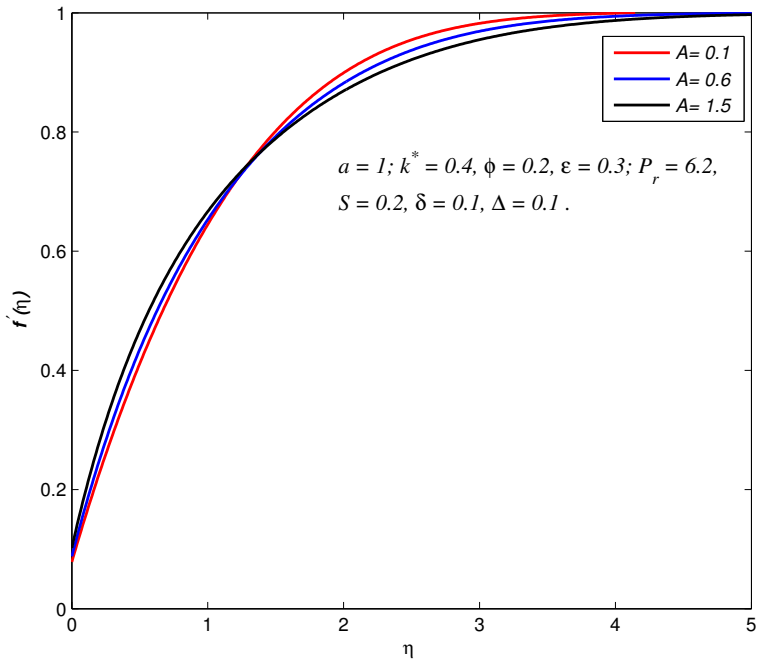

Figure 7. Velocity $f'(\eta)$ profiles for different values of viscosity parameter A.

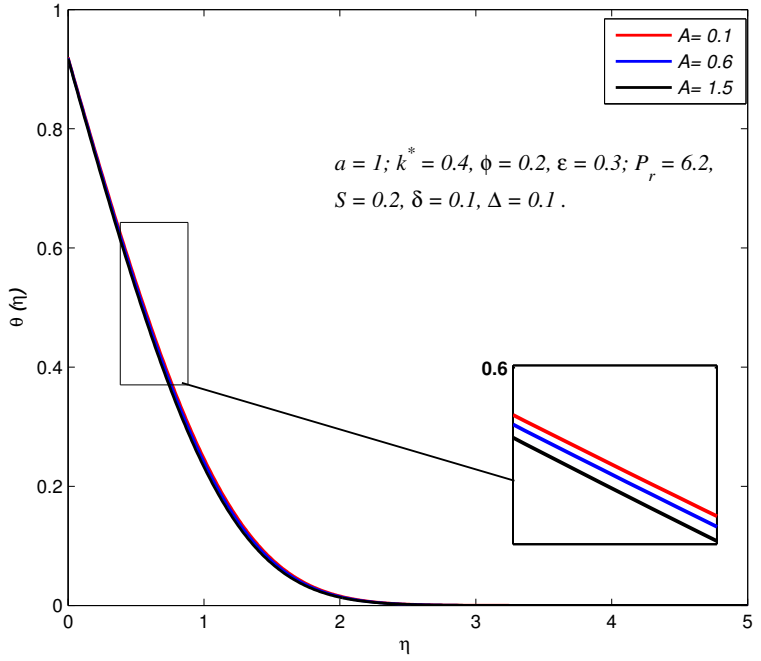

Figure 8. Temperature $\theta(\eta)$ profiles for different values of viscosity parameter A.

Figures 9 and 10 depict the velocity and temperature profiles for the specified values of thermal conductivity parameter ϵ. It is noticed that the variation in ϵ greatly affects the temperature profiles, as compared to the velocity profiles. The variation in velocity profiles show an opposite effect as

the variation in viscosity parameter A, i.e., the increase in thermal conductivity initially causes the decrease in fluid velocity and shows the opposite behavior after the cross-over point; whereas an increase in ϵ results in an increase in thermal conductivity, thereby raising the fluid temperature across the boundary layer. It would also increase the thermal boundary layer thickness.

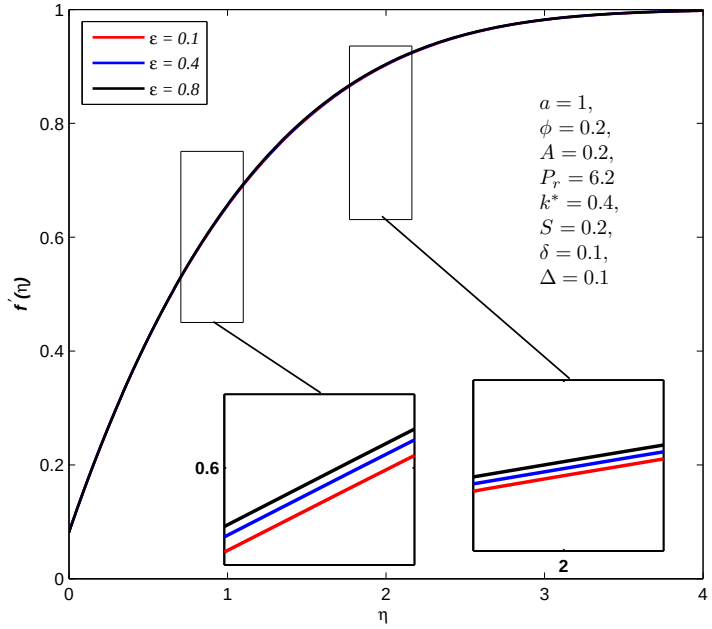

Figure 9. Velocity $f'(\eta)$ profiles for different values of thermal conductivity parameter ϵ.

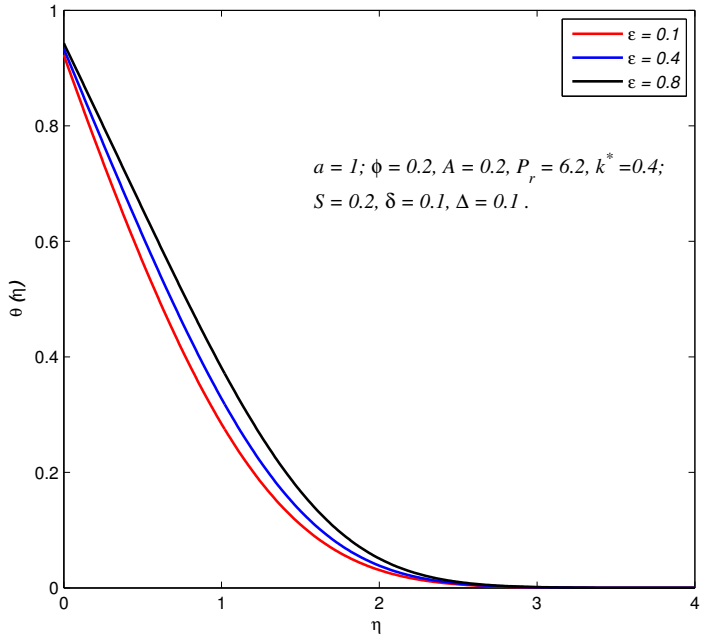

Figure 10. Temperature $\theta(\eta)$ profiles for different values of ϵ.

In Figure 11, the effect of velocity slip parameter δ on the velocity profile of the Cu-water nanofluid is presented. The comparison of the curves shows that the increase in the velocity slip at the boundary increases the fluid velocity within the boundary layer. This is due to the positive value of the fluid velocity adjacent to the surface of the plate and results in a reduction of the momentum boundary

layer thickness. Moreover, the increase in magnitude of the slip parameter allows more fluid to slip past the plate, and accordingly, the flow through the boundary layer will increase. The temperature profiles in Figure 12 show the decrease in temperature and thermal boundary layer thickness with an increase in velocity slip parameter δ.

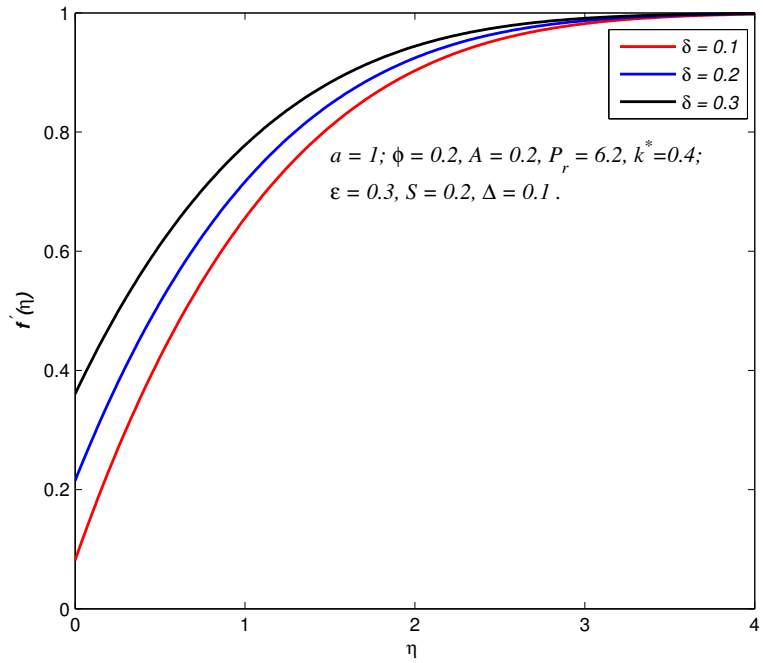

Figure 11. Velocity $f'(\eta)$ profiles for different values of velocity slip parameter δ.

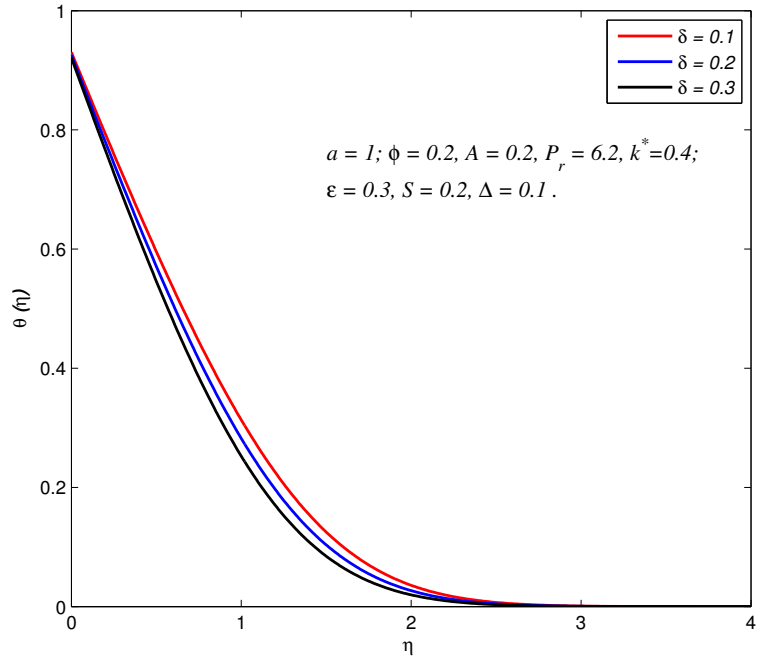

Figure 12. Temperature $\theta(\eta)$ profiles for different values of velocity slip parameter δ.

Figure 13 depicts the decrease in the thickness of the thermal boundary layer with the increase in thermal slip parameter Δ. This is because the increase in the thermal slip parameter causes less transfer of heat from the sheet to the fluid, which leads to a decrease in the boundary layer temperature.

Moreover, the momentum equation is dependent on $\theta(\eta)$, but no significant effect of thermal slip parameter Δ on the velocity profiles is noticed.

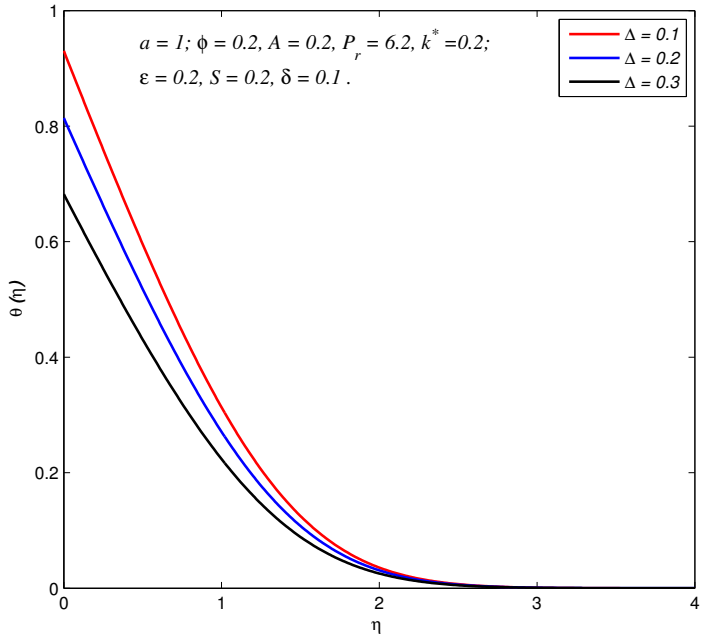

Figure 13. Temperature $\theta(\eta)$ profiles for different values of thermal slip parameter Δ.

The behavior of the velocity and temperature distribution for variation of suction $(S > 0)$ and blowing $(S < 0)$ parameter in the presence of slip conditions at the boundary are plotted in Figures 14−17. For $S > 0$, the fluid velocity increases as the fluid particles are sucked in the porous wall, which in turn reduces the thickness of the momentum boundary layer. On the other hand, for the case of blowing, i.e., $S < 0$, the opposite trend is observed. When suction $S > 0$ is increased, it refers to bringing the fluid close to the wall. This causes a decrease in the temperature profile and also decreases the thermal boundary layer. This entire phenomenon causes an increase in the rate of heat transfer. An opposite trend can be seen for the case of blowing $S < 0$.

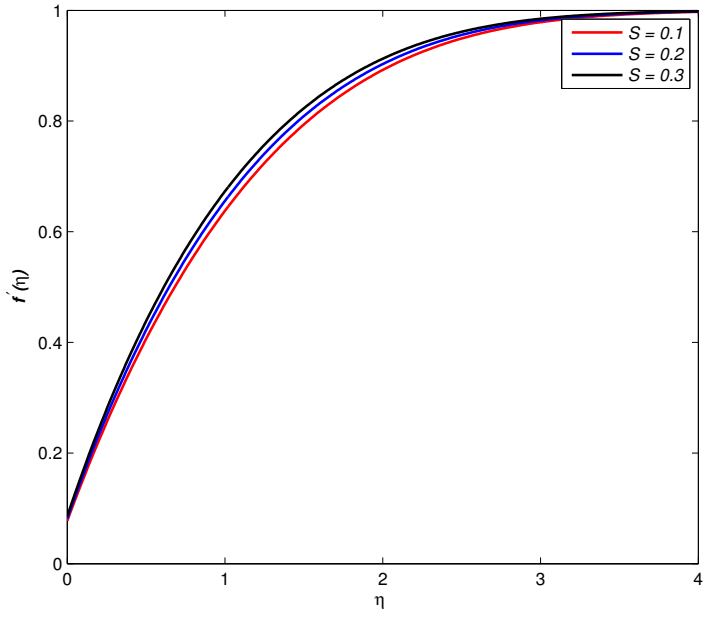

Figure 14. Velocity $f'(\eta)$ profiles for different values of suction parameter $S > 0$.

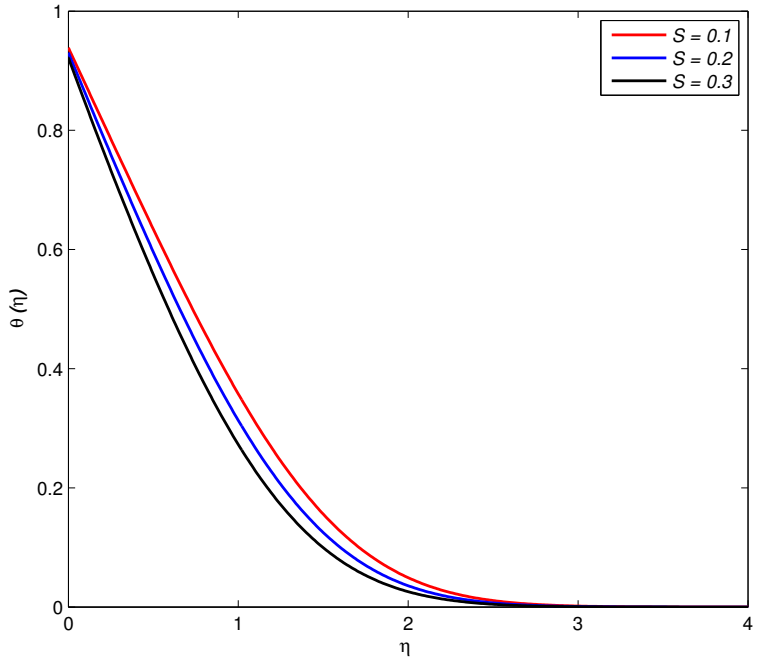

Figure 15. Temperature $\theta(\eta)$ profiles for different values of suction parameter $S > 0$.

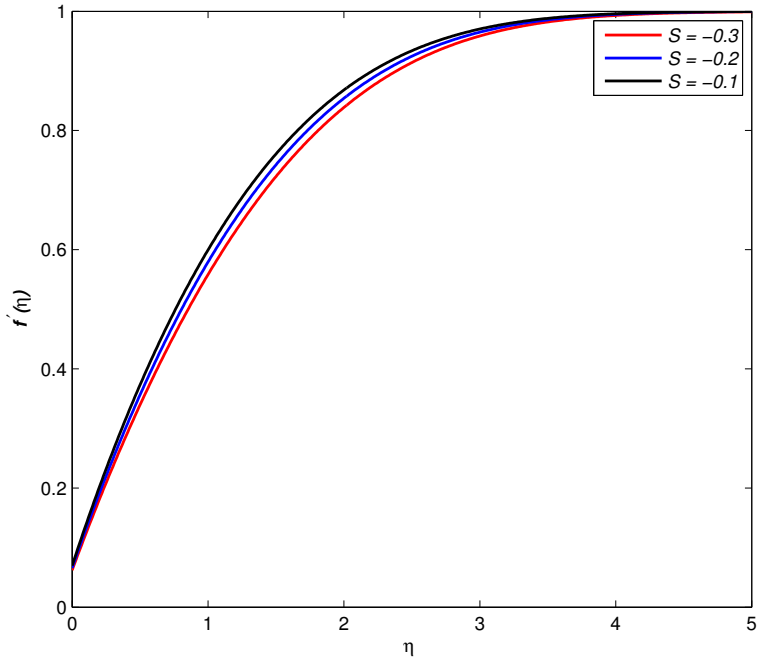

Figure 16. Velocity $f'(\eta)$ profiles for different values of blowing parameter $S < 0$.

The behavior of the skin friction coefficient and Nusselt number with the variation in different thermophysical parameters is shown in Table 2. It is evident that the skin friction coefficient increases with increasing values of permeability parameter k^*, viscosity parameter A, nanofluid volume concentration parameter ϕ and suction parameter S; whereas a decreasing trend is observed for increasing values of thermal conductivity parameter ϵ, velocity slip parameter δ and thermal slip parameter Δ. The increasing values of the skin friction coefficient correspond to the thinning of the velocity boundary layer; whereas the decreasing values of the skin friction coefficient correspond to fluid velocity at the surface approaching the free stream velocity. The negative value of the temperature

gradient at the plate $-\theta'(0)$ is proportional to the rate of heat transfer at the surface of the plate. The rate of heat transfer at the surface is increasing for increasing values of permeability parameter k^*, viscosity parameter A, suction parameter S and velocity slip parameter δ. The rate of heat transfer decreases with the increase in the volume concentration parameter ϕ, the thermal conductivity parameter ϵ and the thermal slip parameter Δ.

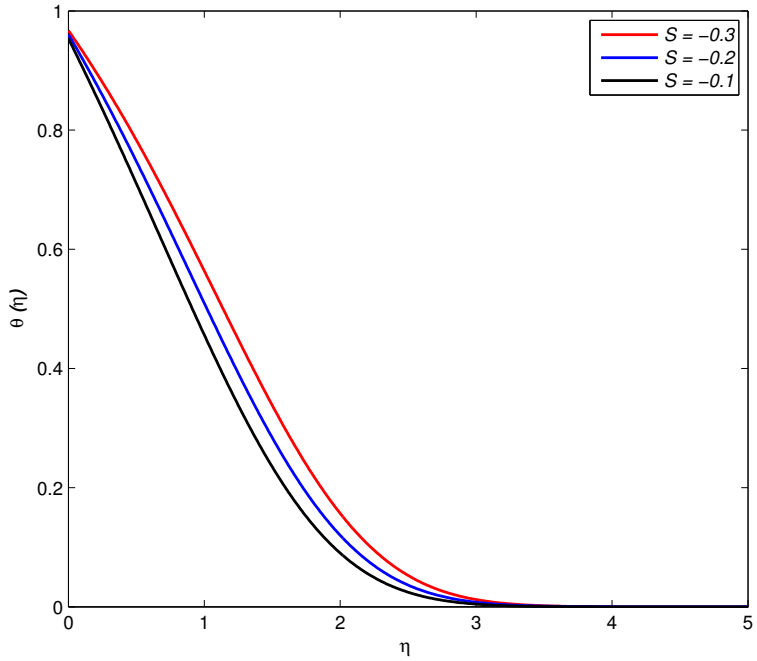

Figure 17. Temperature $\theta(\eta)$ profiles for different values of blowing parameter $S < 0$.

6. Conclusions

In the present research, we investigated the slip effects on the steady flow and heat transfer of nanofluids over a porous sheet embedded in a Darcy-type porous medium. The viscosity and the thermal conductivity of the nanofluids were considered as linear functions of temperature, and wall slip conditions were employed in terms of shear stress. The governing system of equations was reduced to the ordinary differential equations by suitable similarity transformations, and the reduced system was solved numerically using the shooting method. The influence of key thermophysical parameters on the velocity and temperature profiles, as well as on the skin friction coefficient and Nusselt number were presented and discussed through graphs and tables. The present model exploited a number of simplifications in order to focus on the principal effects of permeability, variable viscosity, variable thermal conductivity, nanofluid volume concentration and slip parameters. In our work, we showed that the increase in the permeability of the porous medium, the viscosity of the nanofluids and the velocity slip parameter decreased the momentum and thermal boundary layer thickness and eventually increased the rate of heat transfer; whereas the opposite trend was observed for the increase in the thermal conductivity parameter. The present simplified model can be generalized to reveal the effects of effective dynamic viscosity on the slip flow and heat transfer of nanofluids for the viscosity models proposed by Abu-Nada [45], Khanafer and Vafai [46] and Corcione [47]. Moreover, the analysis can be extended to include the results for different water-based nanofluids, and a comparison can be generated on the heat transfer characteristics of different nanofluids. Clearly, there is an opportunity to consider/extend this problem with non-Newtonian nanofluid models and to perform experimental work on these systems.

Author Contributions: A. A., S. H. and T. A. contributed in the modeling and wrote the paper. S.H. performed the simulations and processed all figures. C.M.K. contributed to the idea and the organization of the research work.

Conflicts of Interest: The authors declare no conflicts of interest.

References

1. Kreith, F.; Boehm, R.F. *Heat and Mass Transfer (Mechanical Engineering Handbook)*; CRC Press: Boca Raton, FL, USA, 1999.
2. Nield, D.; Bejan, A. *Convection in Porous Media*, 3rd ed.; Springer: New York, NY, USA, 2006.
3. Webb, R.; Kim, N. *Principles of Enhanced Heat Transfer*, 2nd ed.; John Wiley: New York, NY, USA, 1994.
4. Maxwell, J. *A Treatise on Electricity and Magnetism*, 2nd ed.; Clarendon Press: Oxford, UK, 1881.
5. Vafai, K. *Handbook of Porous Media*; Marcel Dekker: New York, NY, USA, 2000.
6. Ingham, D.; Pop, I. *Transport Phenomena in Porous Media*; Elsevier: Amsterdam, The Netherlands, 1998.
7. Choi, S.U.S. Enhancing thermal conductivity of fluids with nanoparticles. *ASME Int. Mech. Eng. Congr. Expo.* **1995**, *66*, 99–105.
8. Wang, X.; Xu, X.; Choi, S.U.S. Thermal conductivity of nanoparticle-fluid mixture. *J. Thermophys. Heat Transf.* **1999**, *13*, 474–480.
9. Keblinski, P.; Phillpot, S.R.; Choi, S.U.S.; Eastman, J.A. Mechanisms of heat flow in suspension of nano-sized particles (nanofluids). *Int. J. Heat Mass Transf.* **2002**, *45*, 855–863.
10. Buongiorno, J. Convective transport in nanofluids. *ASME J. Heat Transf.* **2006**, *128*, 240–250.
11. Keblinski, P.; Eastman, J.; Cahill, D. Nanofluids for thermal transport. *Mater. Today* **2005**, *8*, 36–44.
12. Wang, X.Q.; Mujumdar, A.S. Heat transfer characteristics of nanofluids: A review. *Int. J. Therm. Sci.* **2007**, *46*, 1–19.
13. Nield, D.; Kuznetsov, A. Thermal instability in a porous medium layer saturated by a nanofluid. *Int. J. Heat Mass Transf.* **2009**, *52*, 5796–5801.
14. Kuznetsov, A.V.; Nield, D.A. Natural convective boundary-layer flow of a nanofluid past a vertical plate. *Int. J. Therm. Sci.* **2010**, *49*, 243–247.
15. Sun, Q.; Pop, I. Free convection in a triangle cavity filled with a porous medium saturated with nanofluids with flush mounted heater on the wall. *Int. J. Therm. Sci.* **2011**, *50*, 2141–2153.
16. Khan, W.; Aziz, A. Double-diffusive natural convective boundary layer flow in a porous medium saturated with a nanofluid over a vertical plate: Prescribed surface heat, solute and nanoparticle fluxes. *Int. J. Therm. Sci.* **2011**, *50*, 2154–2160.
17. Yadav, D.; Bhargava, R.; Agrawal, G.S. Boundary and internal heat source effects on the on set of darcy-brinkman convection in a porous layer saturated by nanofluid. *Int. J. Therm. Sci.* **2012**, *60*, 244–254.
18. Uddin, M.J.; Khan, W.A.; Ismail, A. Free convection of non-newtonian nano-fluids in porous media with gyrotactic micro organisms. *Transp. Porous Media* **2013**, *97*, 241–252.
19. Servati, V.; Javaherdeh, K.; Ashorynejad, H.R. Magnetic field effects on force convection flow of a nanofluid in a channel partially filled with porous media using lattice boltzmann method. *Adv. Powder Technol.* **2014**, *25*, 666–675.
20. Ahmad, S.; Pop, I. Mixed convection boundary layer flow from a vertical flat plate embedded in a porous medium filled with nanofluids. *Int. Commun. Heat Mass Transf.* **2010**, *37*, 987–991.
21. Cimpean, D.S.; Pop, I. Fully developed mixed convection flow of a nanofluid through an inclined channel filled with a porous medium. *Int. J. Heat Mass Transf.* **2012**, *55*, 907–914.
22. Mahdi, R.A.; Mohammed, H.A.; Munisamy, K.M.; Saeid, N.H. Review of convection heat transfer and fuid fow in porous media with nanofuid. *Renew. Sustain. Energy Rev.* **2005**, *41*, 715–734.
23. Uphill, S.J.; Cosgrove, T.; Briscoe, W.H. Flow of nanofluids through porous media: Preserving timber with colloid science. *Colloids Surf. A Physicochem. Eng. Asp.* **2014**, *460*, 38–50.
24. Zhang, C.; Zheng, L.; Zhang, X.; Chen, G. MHD flow and radiation heat transfer of nanofluids in porous media with variable surface heat flux and chemical reaction. *Appl. Math. Model.* **2015**, *39*, 165–181.
25. Sheikholeslami, M.; Ellahi, R. Electrohydrodynamic Nanofluid Hydrothermal Treatment in an Enclosure with Sinusoidal Upper Wall. *Appl. Sci.* **2015**, *5*, 294–306.
26. Reddy, J.V.R.; Sugunamma, V.; Sandeep, N.; Sulochana, C. Influence of chemical reaction, radiation and rotation on MHD nanofluid flow past a permeable flat plate in porous medium. *J. Niger. Math. Soc.* **2016**, *35*, 48–65.

27. Luk, J.; Mutharasan, R.; Apelian, D. Experimental observations of wall slip: Tube and packed bed flow. *Ind. Eng. Chem. Res.* **1987**, *26*, 1609–1616.
28. Kalyon, D.M. Apparent slip and viscoplasticity of concentrated suspensions. *J. Rheol.* **2005**, *49*, 621–640.
29. Khan, W.A.; Khan, Z.H.; Rahi, M. Fluid flow and heat transfer of carbon nanotubes along a flat plate with navier slip boundary. *Appl. Nanosci.* **2014**, *4*, 633–641.
30. Zheng, L.; Niu, J.; Zhang, X.; Gao, Y. MHD Flow and Heat Transfer over a Porous Shrinking Surface with Velocity Slip and Temperature Jump. *Math. Comput. Model.* **2012**, *56*, 133–144.
31. Zheng, L.; Zhang, C.; Zhang, X.; Zhang, J. Flow and radiation heat transfer of a nanofluid over a stretching sheet with velocity slip and temperature jump in porous medium. *J. Frankl. Inst.* **2013**, *350*, 990–1007.
32. Uddin, M.J.; Khan, W.A.; Amin, N.S. g-jitter mixed convective slip flow of nanofluid past a permeable stretching sheet embedded in a darcian porous media with variable viscosity. *PLoS ONE* **2014**, *9*, e99384.
33. Noghrehabadi, A.; Pourrajab, R.; Ghalambaz, M. Effect of partial slip boundary condition on the flow and heat transfer of nanofluids past stretching sheet prescribed constant wall temperature. *Int. J. Therm. Sci.* **2012**, *54*, 253–261.
34. Bhaskar, N.R.; Poornima, T.; Sreenivasulu, P. Influence of variable thermal conductivity on MHD boundary layer slip flow of ethylene-glycol based Cu nanofluids over a stretching sheet with convective boundary condition. *Int. J. Eng. Math.* **2014**, *2014*, 905158.
35. Noghrehabadia, A.; Ghalambaza, M.; Ghanbarzadeha, A. Effects of variable viscosity and thermal conductivity on natural-convection of nanofluids past a vertical plate in porous media. *J. Mech.* **2014**, *30*, 265–275.
36. Uddin, M.J.; Pop, I.; Ismail, A.I.M. Free convection boundary layer flow of a nanofluid from a convectively heated vertical plate with linear momentum slip boundary condition. *Sains Malays.* **2012**, *4*, 1475–1482.
37. Ibrahim, W.; Shankar, B. MHD boundary layer flow and heat transfer of a nanofluid past a permeable stretching sheet with velocity, thermal and solutal slip boundary conditions. *Comput. Fluids* **2013**, *75*, 1–10.
38. Ellahi, R. The effects of MHD and temperature dependent viscosity on the flow of non-Newtonian nanofluid in a pipe: analytical solutions. *Appl. Math. Model.* **2013**, *37*, 1451–1467.
39. Sharma, R.; Ishak, A. Second order slip flow of cu-water nanofluid over a stretching sheet with heat transfer. *WSEAS Trans. Fluid Mech.* **2014**, *9*, 26–33.
40. Mohyuddin, S.T.; Khan, U.; Ahmed, N.; Hassan, S.M. Magnetohydrodynamic Flow and Heat Transfer of Nanofluids in Stretchable Convergent/Divergent Channels. *Appl. Sci.* **2015**, *5*, 1639–1664.
41. Pandey, A.K.; Kumar, M. Effect of viscous dissipation and suction/injection on MHD nanofluid flow over a wedge with porous medium and slip. *Alex. Eng. J.* **2016**, doi:10.1016/j.aej.2016.08.018.
42. Arunachalam, M.; Rajappa, N.R. Forced convection in liquid metals with variable thermal conductivity and capacity. *Acta Mech.* **1978**, *31*, 25–31.
43. Bhattacharyya, K.; Layek, G.C.; Gorla, R.S.R. Boundary layer slip flow and heat transfer past a stretching sheet with temperature dependent viscosity. *Therm. Energy Power Eng.* **2013**, *2*, 38–43.
44. Shankar, B.; Yirga, Y. Unsteady heat and mass transfer in mhd flow of nanofluids over stretching sheet with a non-uniform heat source/sink. *World Acad. Sci. Eng. Technol. Int. J. Math. Comput. Stat. Nat. Phys. Eng.* **2013**, *7*, 12.
45. Abu-Nada, E. Effects of variable viscosity and thermal conductivity of Al_2O_3–water nanofluid on heat transfer enhancement in natural convection. *Int. J. Heat Fluid Flow* **2009**, *30*, 679–690.
46. Khanafer, K.; Vafai, K. A critical synthesis of thermophysical characteristics of nanofluids. *Int. J. Heat Mass Transf.* **2011**, *54*, 4410–4428.
47. Corcione, M. Empirical correlating equations for predicting the effective thermal conductivity and dynamic viscosity of nanofluids. *Energy Convers. Manag.* **2011**, *52*, 789–793.